UCRL-JRNL-212861

LAWRENCE
LIVERMORE
NATIONAL
LABORATORY

Rapid Assessment of the Influence of Solution pH, Anion Concentration and Temperature on the Dissolution of Alloy 22

J. J. Gray, J. R. Hayes, G. E. Gdowski, B. E. Viani, C. A. Orme

June 10, 2005

Journal of the Electrochemical Society

This document was prepared as an account of work sponsored by an agency of the United States Government. Neither the United States Government nor the University of California nor any of their employees, makes any warranty, express or implied, or assumes any legal liability or responsibility for the accuracy, completeness, or usefulness of any information, apparatus, product, or process disclosed, or represents that its use would not infringe privately owned rights. Reference herein to any specific commercial product, process, or service by trade name, trademark, manufacturer, or otherwise, does not necessarily constitute or imply its endorsement, recommendation, or favoring by the United States Government or the University of California. The views and opinions of authors expressed herein do not necessarily state or reflect those of the United States Government or the University of California, and shall not be used for advertising or product endorsement purposes.

Updated October 14, 2003

Rapid assessment of the influence of solution pH, anion concentration and temperature on the dissolution of Alloy 22

J.J. Gray[z], J.R. Hayes, G.E. Gdowski, B.E. Viani, C. A. Orme

Lawrence Livermore National Laboratory, Livermore CA 94550, USA

Abstract

We introduce an acid titration technique for the rapid characterization of the influence of solution pH, anion (such as chloride) concentration and temperature on the dissolution of metals. We demonstrate the technique with the characterization of the dissolution of alloy 22 (Ni-22Cr-13Mo-3W-3Fe) exposed to chloride-containing hydrochloric, sulfuric and nitric acid environments as a function of pH (from pH 5 to pH −1) and temperature (25 – 90°C). A combination of electrochemical techniques (electrochemical impedance spectroscopy and linear polarization resistance) and atomic force microscopy are used to characterize the influence of the various solutions on the dissolution of alloy 22. In solutions containing hydrochloric and sulfuric acids, a critical temperature exists for passive film breakdown on alloy 22 for all environments tested. Below the critical temperature, corrosion rates are less than 1μm/year. Above the critical temperature, the effect of temperature on dissolution rates is a function of both the pH and chloride content of the solution. In nitric acid containing solutions, the presence of nitrates promotes a stable passive oxide film that inhibits dissolution in all environments tested.

[z] Contact author: gray46@llnl.gov

Introduction

Nickel-based alloys are employed in a wide range of applications where long lifetimes are vital such as in implant materials and nuclear waste storage. The robustness of alloys in these types of environments is due to the formation of a protective "passive" oxide film at the alloy interface. The nature and composition of these oxide films depends markedly on the alloy composition and the pH, temperature and electrolyte composition of the formation environment. Alloys can be tailored to fit a specific set of environmental conditions by selection of constituent elements that have strengths that compensate in the areas where other elements fail. For example, for Ni-Cr-Mo alloys, it is generally well established that the Mo provides resistance against reducing acidic environments, Cr against oxidizing conditions, Cr and Mo against localized attack, and Ni, Cr, and Mo against stress corrosion cracking due to chloride ions[1]. This combination of corrosion resistance in both reducing and oxidizing environments make these alloys particularly well suited as long-term storage materials. As a result, the Ni-Cr-Mo alloy, alloy 22 (Ni-Cr22-Mo13-W3-Fe3), is the candidate material for the outer wall of nuclear waste packages at the Yucca Mountain nuclear waste repository (Nevada, USA). Over the past decade, a number of studies have been undertaken to characterize its general and localized corrosion properties[2-5]. These studies demonstrate that alloy 22 is exceptionally corrosion resistant in a broad range of concentrated brines including chloride, fluoride, carbonate, sodium and calcium with pH values ranging from ~2.7 to 13 and temperatures from 25 to 120°C [6]. To date, little work has been done to characterize the alloys susceptibility to breakdown in aggressive solutions that may exist in occluded volumes

such as crevices where increased corrosion rates are generally considered to occur by a gradual increase in the acidity and anion (eg. Cl^-) concentration[7-9]. In this paper, we test the passivity of alloy 22 over a range of pH and anion concentration broad enough to encompass the aggressive solutions that may exist in these localized environments. To characterize the dissolution of alloy 22, we measure film thicknesses (as determined by electrical impedance spectroscopy (EIS)) and dissolution rates (as determined by linear polarization resistance (LPR)) at 25, 60 and 90°C in 1 and 4 molal sodium chloride-containing hydrochloric, sulfuric and nitric acid solutions. After exposure to the various solutions, we utilize topographic maps of the surface from atomic force microscopy (AFM) to elucidate the mechanisms of dissolution.

Experimental

Alloy 22 samples were machined into 5/8" diameter discs approximately 1/8" thick and then mechanically polished by successively finer polishing compounds down to 0.02 micron colloidal silica. The exposed area of the sample disc during electrochemical testing was approximately 0.7 cm^2. Electrochemical tests were performed in a standard three-electrode electrochemical cell placed in a heating mantel. The mantel heating element was referenced to a thermocouple directly immersed in the cell solution and controlled through a closed loop temperature controller. A volume of 900mL of solution was initially placed in the cell. The cell was equipped with a gas stream flowing 99.999% pure nitrogen used for the duration of each experiment to deaerate the solution. The nitrogen stream was immersed directly into the aqueous solutions, which also aides in stirring the solutions. The cell also had a condenser tube connected to a chilled water

line held at 15°C to prevent evaporation of the electrolyte, a luggin probe salt bridge connected to a saturated Ag/AgCl (SSC) reference electrode, and either a platinum or graphite counter electrode.

All electrochemical measurements were performed using a commercial potentiostat / galvanostat / zero resistance ammeter (Gamry Instruments, Warminster, PA). For LPR and EIS measurements, the specimens were polarized at a peak-to-peak voltage amplitude of 10 mV relative to the instantaneous open circuit potential (OCP). Impedance frequency-dependence was analyzed over a range of 10^{-2} to 10^{5} Hz. Ex situ AFM images were acquired using a Digital instruments Inc., Dimension 3100 Scanning Probe Microscope (Santa Barbara, CA) with a large scan stage. Samples were imaged in contact mode at a scan rate of 1Hz.

Titration technique

A schematic of the acid concentration as a function of time for a representative titration experiment is illustrated in Fig. 1. Before the specimens are loaded, the solution is deaerated with nitrogen gas for one hour and the temperature and pH values are recorded. Subsequently, the sample is immersed in the electrochemical cell. An OCP measurement is performed for two hours while the sample surface comes to equilibrium with the solution. This appears to be a sufficient conditioning period, since in three-day measurements (not shown here) we found very little change after the first hour in acidic conditions. This wait time may be insufficient under neutral conditions and thus the OCP values for first few data points in the titrations may be underestimated. Following the OCP measurement, EIS and three consecutive LPR measurements are used to

characterize the passive film properties and alloy 22 dissolution rates. Upon completion of the LPR measurements, a programmable dual syringe pump is used to withdraw a precise volume of solution from the electrochemical cell and subsequently inject the same volume of acid (from an external reservoir) into the cell. The external reservoir contains sodium chloride at a concentration nominally equal to that in the reaction cell. Consequently, the concentration of sodium chloride in the cell remains nominally constant (within 10 percent) while the overall acid concentration increases. Once the syringe pump dispenses acid into the cell, an OCP measurement is once again performed followed by EIS and LPR. This process is repeated until the pH is well below zero. All titrations were performed in sodium chloride solutions of 1 and 4m. The chloride concentrations remain fixed (+/- 10%) throughout the titration for pure sulfuric and nitric titrations except when HCl is one of the titrants, the total chloride concentration increases.

pH calculation

Although the acids used are highly dissociated in dilute solutions at room temperature, ion association can be significant for concentrated solutions at elevated temperature, Hence, the stoichiometric proton concentration (stoichiometric pH) is not suitable for comparing the effects of different acids on corrosion rates. The pH values reported in this paper were calculated using Pitzer ion interaction theory[10] using the geochemical modeling software EQ3/6[11]. We used a set of internally consistent ion interaction parameters for the systems H_2SO_4, NaCl, HNO_3, HCl that were based on reported data[12-18] and recalculated to be consistent with standard Pitzer model parameters [18] and with the temperature function used in EQ3/6. The pH calculated by the Pitzer

approach is based on the single ion activity coefficient for the proton. In order to be consistent with pH definitions used for low ionic strength fluids, we have scaled activity coefficients according to the NBS (National Bureau of Standards) convention using the Bates-Guggenheim equation[19]. We simulated the experimental titration by using appropriate additions of acids and background electrolytes while calculating pH. The EQ3/6 output of pH vs. stoichiometric hydrogen molality was then interpolated to obtain pH at the experimental molalites at which pH was measured.

Results

Figures 2 through 4 compare corrosion rates and open circuit potentials as a function of pH for the different acids at 60°C and 90°C in a 1m NaCl base, and 90°C in a 4m NaCl base, respectively. A convenient metric that is generally used to correlate corrosion rates with breakdown is 100 μm/yr[9]. The pH values where the corrosion rates increase above 100 μm/yr marks the breakdown of the passive film of alloy 22. In hydrochloric and sulfuric acids, the critical pH values at 60°C in 1m NaCl (Fig. 2) are near pH ~ 0.5. At higher temperature, 90° (Fig. 3), the critical pH values are shifted to pH 0.75 and 0.6 for hydrochloric and sulfuric solutions, respectively. Additionally, corrosion rates in hydrochloric are consistently higher than for sulfuric acids at 90°C for all tested pH. In more concentrated, 4m NaCl solutions (Fig. 4), the critical pH value is approximately 2.5 for both hydrochloric and sulfuric solutions. The breakdown of the passive film is also evident in the OCP curves. At the same pH that the corrosion rates increase, the drop in the OCP corresponds to an activation stage where passivity breaks down[8]. In nitric acid, corrosion rates remain very low for all pH values tested, and in the

low pH range, where hydrochloric and sulfuric acid solutions show approximately no OCP change, the OCP steadily increases.

Electrical Impedance Measurements

EIS measurements were made to characterize the influence of the acids on passive film thickness. Thicknesses were calculated by considering the barrier layer as a parallel-plate capacitor, such that

$$L_{ss} = \varepsilon_0 \varepsilon / C_f \tag{1}$$

where, L_{ss} is the steady-state passive layer thickness, ε is the dielectric constant of the oxide (assumed to be that of Cr_2O_3, $\varepsilon = 30$), ε_0 is the permittivity of free space and C_f is the capacitance of the passive film. The steady state assumption is considered valid because the EIS measurements were made two hours after the addition of acid and the OCP was constant after the first hour. Passive film thickness values were calculated by fitting the imaginary component of the interfacial impedance at high frequencies to equivalent circuits[5]. Film thicknesses for all acids in 1m NaCl at 60°C are plotted vs. pH in Fig. 5. For hydrochloric and sulfuric acids, the pH values where the corrosion rates rapidly increase correlate to the pH where L_{ss} decreases to near zero. Conversely, in the presence of nitric acid, the oxide film grows thicker with decreasing pH.

Ex situ morphology with AFM

In Figs. 6 and 7, we show AFM images of the surface morphology following titration experiments in 1m NaCl at 60 and 90°C, respectively. To estimate the amount of alloy removed during the titration experiment, we time-integrate the corrosion rate

obtained from LPR measurements. after titration at 60°C, the total alloy penetration depth is approximately 225μm in both sulfuric and hydrochloric acid exposed samples. In nitric acid, the total penetration depth is 0.26μm. However, due to the fact that in nitric acid, the passive film thickens with increasing pH, the corrosion rates measured most likely correspond to a combination of charge transfer for metal ions forming metal oxide complexes and metal-oxide dissolution at a ratio which leads to an overall thickening of the passive film. At 90°C, AFM images were taken after approximately 1260μm of alloy were removed in H_2SO_4 and 2000μm in HCl. The total penetration depth after titration in nitric acid at 90°C was approximately 4.3μm.

The AFM micrographs in Figs. 6 and 7 indicate that the mode of metal dissolution differs in the different acid types. At 60°C, the dissolution mechanisms are similar for samples exposed to HCl and H_2SO_4, each showing preferential etching depending on the crystallographic orientation of the grain according to the surface atom density with etch rates most likely scaling with orientation[20,21]. Overall this leads to a roughening of the surfaces and in particular, preferential grain etching leads to large depressed regions 200-500nm deep and 10's of microns wide. In contrast, the nitric acid exposed specimen shows a slightly porous structure indicative of a thickened oxide film.

At 90°C, samples exposed to HCl and H_2SO_4 show very different dissolution mechanisms. As in the case when the temperature is 60°C, the sample exposed to HCl shows preferential etching dependent on the orientation of the grain. The dissolution process is associated with the underlying step structure of the alloy 22 surface. The very straight step edges are aligned in various directions, most likely along crystallographic

planes. From Fig. 6a, the H_2SO_4 exposed samples also show preferential etching but with a scalloped appearance along the dissolution step directions. Samples exposed to nitric acid at 90°C show mild intergranular attack and some anisotropic dissolution processes.

Discussion

Effect of chloride ion concentration

From a comparison of the corrosion rate vs. pH curves in Figs. 3 and 4, the chloride concentration plays a significant role in the breakdown kinetics of the passive film of alloy 22. In hydrochloric acid, with a four-fold increase in the base chloride concentration, the pH at which the passive film breaks down shifts from 0.75 to 2.5. Likewise, in sulfuric acid, the breakdown pH shifts from 0.6 to 2.5 for the same chloride concentration increase. Several mechanisms have been proposed to explain the effects of chloride on passive film dissolution, all of which support the assumption that initially chloride is adsorbed on the passive film surface and/or the metallic surface. Following chloride adsorption, three mechanisms have been rationalized: (1) Penetration of chloride ions into the passive film resulting in the accumulation of Cl^- ions at the metal interface which causes film breakdown by the formation of metal chlorides[22]. (2) Complexation and thinning of the passive film from chloride ions adsorbed on the oxide surface complexing with the surface cations. A high solubility of the complex would enhance the dissolution and cause thinning of the passive film[23]. (3) The presence of Cl^- ions prevents repassivation of locally depassivated surfaces and thus causes pitting[24].

To elucidate which mechanism(s) is (are) responsible for the breakdown of passive films of alloy 22 at low pH, we analyzed the films using XPS. Ex situ XPS (not

shown here) analysis of samples immersed in 1m NaCl at pH 3 and 90°C (passive film still in tact) show no evidence of chlorine ions in the passive film. Conversely, the XPS data shows contributions primarily from Cr(III) species with a lesser concentration of Mo species. Similar observations have been made for other nickel based alloys in low pH environments[4]. The EIS data in Fig. 5 indicate that in hydrochloric and sulfuric acids, as the pH is lowered the passive film becomes increasingly thinner until it eventually is near zero. This suggests that surface oxide metal-chloride complexation leading to a thinning of the oxide layer is a likely mechanism for dissolution in the presence of chlorides (mechanism 2). Under this assumption, an increase in the base concentration of chloride accelerates the thinning of the oxide by increasing the rate of dissolution of metal chlorides directly from the passive film. Ex situ AFM images of alloy 22 samples removed from solution immediately following passive film breakdown show no pitting morphology. Together, these observations suggest that mechanism (2) is favored over (1) and (3) in describing the role that chloride plays on passive film breakdown of alloy 22.

Effect of sulfate ion concentration

From Fig. 2a, sulfate appears to inhibit alloy 22 dissolution as is illustrated by the decrease in dissolution rate at low pH at 90°C. The morphology of alloy 22 after titration in sulfuric acid at 90°C (Fig. 6a) suggests that the dissolution inhibition may be attributed to a step-pinning mechanism leading to slower dissolution of specific step orientations. In Fig. 8a, which is a more detailed view of the dissolution mechanism, each of the metal grains in the image has fluctuating steps that are approximately aligned in one orientation. Moreover, the steps have a scalloped appearance that often occurs when adsorbates impede the local motion of the step, eventually leading to the bunching of

steps. Steps that do not have the proper chemistry, shape or size to allow adsorbate binding will move (dissolve) unimpeded resulting in a morphology that is dictated by the slower moving pinned steps. In the case of alloy 22 in sulfuric acid at 90°C, this suggests that step-specific sulfate binding plays a role in the inhibitory effect observed at low pH in Fig. 2. Similarly, Uhlig et al. reported that competitive adsorption of anions with Cl-- ions at active sites was responsible for an observed corrosion inhibition of stainless steels in chloride media[25,26]. In contrast to the dissolution inhibition observed at 90°C, at 60°C (Fig. 3a) there is no observed inhibition effect due to sulfuric acid. Additionally, from the AFM images in Fig. 6, the dissolution mechanisms for HCl and H_2SO_4 both proceed by step flow etching with rates that depend on the crystallographic grain orientation. The initiation of sulfate inhibition at higher temperature may suggest that the step-pinning process is favored at higher alloy dissolution rates. Vogt et al. observed a similar behavior for Cu dissolution in HCl and H_2SO_4. At sufficiently low rates, step flow dissolution of Cu(100) is observed in both HCl and H_2SO_4. Conversely, at higher rates, the HCl exposed Cu oriented steps are preserved, while in H_2SO_4, significant step roughening is observed[27]. In the case of alloy 22, at 60°C the dissolution rates appear to be low enough that both HCl and H_2SO_4 undergo step flow dissolution. Whereas, at 90°C, the dissolution rates are sufficiently high that step roughening (due to step-pinning) becomes an inhibiting factor in the dissolution process.

Effect of nitrate ion concentration

Figs. 2-4 show that nitrate in chloride solutions inhibits alloy 22 dissolution as compared to pure chloride and chloride plus sulfate solutions. The inhibition process can be attributed to the properties of the passive oxide film in response to the presence of nitrates. The nitrate ions in solution are consumed by the passive oxide film by the reaction $HNO_3 + H^+ + e^- \rightarrow NO_2 + H_2O$[28]. The rate of the reaction increases with increasing concentration of HNO_3. Consequently, the addition of HNO_3 accelerates the reaction concurrent with an increase in the open circuit potential. As a result, spontaneous passivation of the alloy 22 surface occurs changing it from active to passive (Fig. 2b-4b)[28]. During passivation, the oxide film appears to thicken with decreasing pH (Fig. 5). The appearance of two active regions in the corrosion rate vs. pH curve in 4m NaCl (Fig. 4) is most likely due to an active/passive transition at higher pH (pH ~ 1.5) and transpassive dissolution at low pH (pH < 0). This result will be discussed in more detail elsewhere[29]. The AFM micrograph in Fig. 7c, indicates that the dissolution that occurs in nitric acid is dependent on the crystallographic orientation of the polycrystalline alloy 22 surface at 90°C. Whereas, at 60°C the measured corrosion rate most likely contributes to a thickening of the passive film, which leads to the porous oxide structure in the micrograph of Fig. 6c.

Effect of temperature and pH on passive film breakdown

To characterize the dependence of passive film breakdown on temperature and pH, in Fig. 9, we show corrosion rates as a function of temperature for pH values of -0.5, 0.0 and 0.5 in sulfuric acid with 1m NaCl. Above pH 0.5, there is no temperature dependence on the corrosion rate of alloy 22, with dissolution rates below 1μm/yr in all

solutions tested. At pH 0.0 and –0.5 the corrosion rates scale linearly with increasing temperatures above a critical temperature, T_{crit} (see fig 9 inset, which shows corrosion rate vs. temperature in a pH –0.5 1m NaCl sulfuric acid solution). By fitting the slope of the corrosion rate vs. temperature we can quantify the relationship. In H_2SO_4, alloy 22 corrosion rates increase by 80 (μm/yr)/°C and 265 (μm/yr)/°C for pH 0.0 and -0.5, respectively, above T_{crit} ~ *50°C*. Similarly, in HCl (not shown), corrosion rates are 180 (μm/yr)/°C at pH 0.0 and 305 (μm/yr)/°C at pH -0.5. Mirolyubov et al also observe linear increases in corrosion rates with increasing temperatures for 304 stainless steels. At higher Cl- concentrations (4m) the critical temperature is shifted to T_{crit} ~ *xx and below the critical pH (2.5) the corrosion rates scale linearly with temperature at xx. Above the critical pH there is no temperature dependence on the corrosion rate of alloy 22.*

The existence of a critical temperature coupled with the chloride model of dissolution indicates that the critical temperature is most likely related to the overcoming of an energy activation barrier for the complexation of metal oxide species with chloride at the passive film solution interface.

Conclusions

A critical temperature exists for passive film breakdown on alloy 22 for all environments tested. Below the critical temperature, corrosion rates are less than 1μm/year. Above the critical temperature, the effect of temperature on dissolution rates is a function of both the pH and chloride content of the solution. When the solution pH is greater than or equal to the critical pH for passive film breakdown, there is little to no

temperature dependence on the corrosion rate of alloy 22. Conversely, at values less than the critical pH, corrosion rates scale linearly with temperature. In general, higher chloride concentrations lead to passive film breakdown at higher pH in both sulfuric and hydrochloric acid solutions. EIS, XPS and AFM results demonstrate that the likely influence of chloride during dissolution is the complexation of chloride and the metal species in the passive film leading to a progressively thinner film. Finally, in nitric acid, dissolution is inhibited by the formation of a thick passive film.

Acknowledgements

This work was performed under the auspices of the U.S. Department of Energy by University of California, Lawrence Livermore National Laboratory under Contract W-7405-Eng-48.

References

[1] W. Z. Friend, *Corrosion of Nickel and Nickel-base Alloys* (Wiley-Interscience, New York, 1980).
[2] S. D. Day, M. T. Whalen, K. J. King, G. A. Hust, L. L. Wong, J. C. Estill, and R. B. Rebak, Corrosion **60,** 804-814 (2004).
[3] K. J. Evans, A. Yilmaz, S. D. Day, L. L. Wong, J. C. Estill, and R. B. Rebak, Jom **57,** 56-61 (2005).
[4] A. C. Lloyd, D. W. Shoesmith, N. S. McIntyre, and J. J. Noel, Journal of the Electrochemical Society **150,** B120-B130 (2003).
[5] D. D. Macdonald, A. Sun, N. Priyantha, and P. Jayaweera, Journal of Electroanalytical Chemistry **572,** 421-431 (2004).
[6] G. M. Gordon, Corrosion **58,** 811-825 (2002).
[7] D. Tromans and L. Frederick, Corrosion **39,** 305-312 (1983).
[8] J. W. Oldfield and W. H. Sutton, British Corrosion Journal **13,** 104-111 (1978).
[9] J. W. Oldfield and W. H. Sutton, British Corrosion Journal **13,** 13-22 (1978).
[10] *Activity Coefficients in Electrolyte Solutions*; *Vol. 2*, edited by K. S. Pitzer (CRC Press, Boca Raton, Florida, 1991).

[11] *Chemical Modeling of Aqueous Systems II*; *Vol.*, edited by T. J. Wolery, K. J. Jackson, W. L. Bourcier, C. J. Bruton, B. E. Viani, and J. M. Delany (Washington D.C., 1989).
[12] D. Archer, Journal of Physical and Chemical Reference Data **29,** 1141 (2000).
[13] J. P. Greenberg, and N. Moller, Geochimica Cosmochimica Acta **53,** 2503 (1989).
[14] H. F. Holmes, J.M. Busey, J.M. Simonson, R.E. Mesmer, D.G. Archer, and R.H. Wood, Journal of Chemical Thermodynamics **19,** 863 (1987).
[15] S. He, and J.W. Morse, Geochimica Cosmochimica Acta **57,** 3533 (1993).
[16] H. F. Holmes, and R.E. Mesmer, Journal of Chemical Thermodynamics **26,** 581 (1994).
[17] R. T. Pabalan, and K.S. Pitzer, Geochimica Cosmochimica Acta **51,** 829 (1987).
[18] J. A. Rard, and A.M. Wijesinghe, Journal of Chemical Thermodynamics **35,** 439 (2003).
[19] R. G. Bates, *Determination of pH* (Wiley and Sons, N.Y., 1964).
[20] J. J. Gray, B.S. El-Dasher, and C.A. Orme, in preparation.
[21] C. A. Schuh, K. Anderson, and C. Orme, Surface Science **544,** 183-192 (2003).
[22] W. P. Yang, D. Costa, and P. Marcus, Journal of the Electrochemical Society **141,** 111-116 (1994).
[23] H.-H. Strehblow, in *Corrosion Mechanisms in Theory and Practice*, edited by P. Marcus, J. Oudar (Marcel Dekker, New York, 1995), p. 201-237.
[24] N. Sato, Electrochim. Acta **16,** 1683 (1971).
[25] H. P. Leckie, and H.H. Uhlig, J. Electrochem. Soc. **113,** 1262 (1966).
[26] H. H. Uhlig, and , J.R. Gilman, Z. Phys. Chem **226,** 127 (1964).
[27] M. R. Vogt, A. Lachenwitzer, O. M. Magnussen, and R. J. Behm, Surface Science **399,** 49-69 (1998).
[28] V. P. Razygraev, R. S. Balovneva, E. Y. Ponomareva, and M. V. Lebedeva, Protection of Metals **26,** 43-48 (1990).
[29] J. J. Gray, J.R. Hayes, G.E. Gdowski, B.E. Viani, and C.A. Orme, in preparation.

Figures

Fig.1

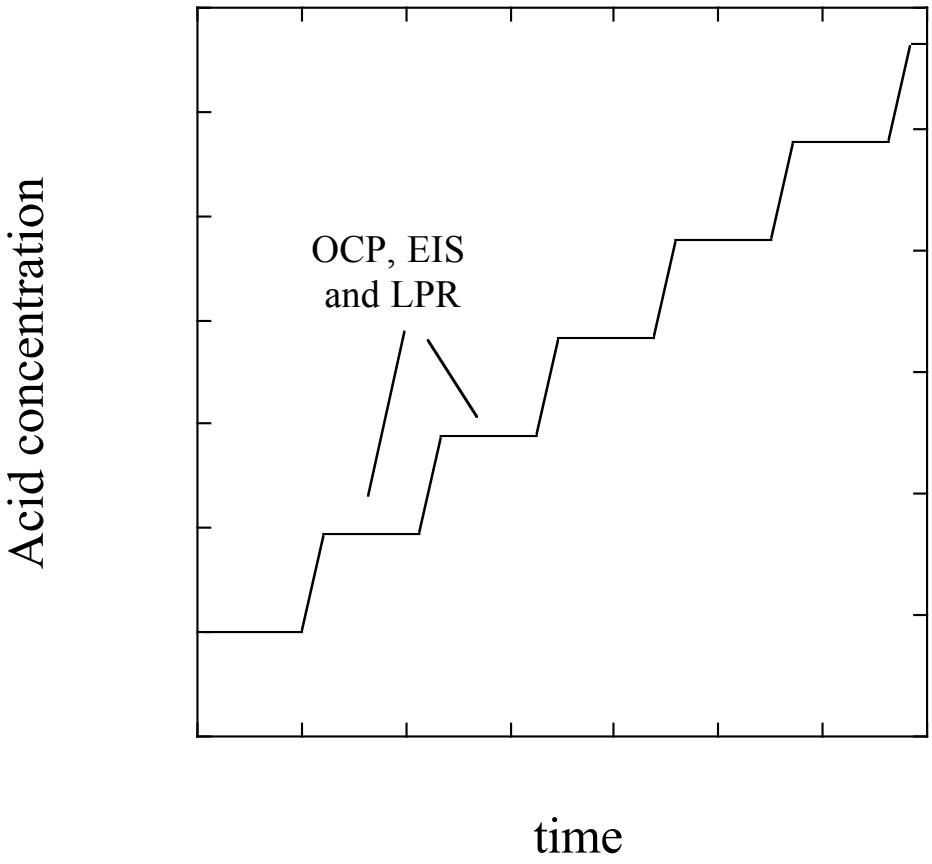

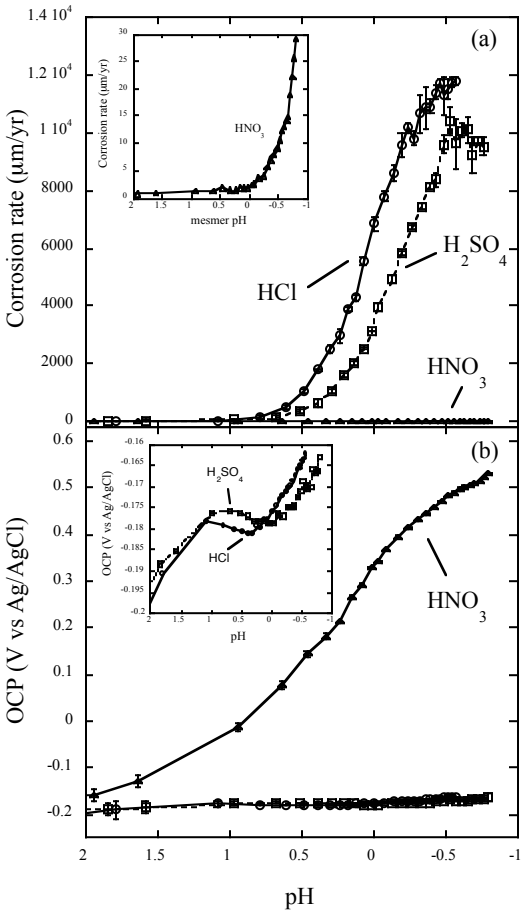
(a)
Corrosion rate (µm/yr)
HCl
H2SO4
HNO3
Corrosion rate (µm/yr)
mesmer pH
(b)
OCP (V vs Ag/AgCl)
HNO3
H2SO4
HCl
OCP (V vs Ag/AgCl)
pH
pH

Fig.2

Fig.3.

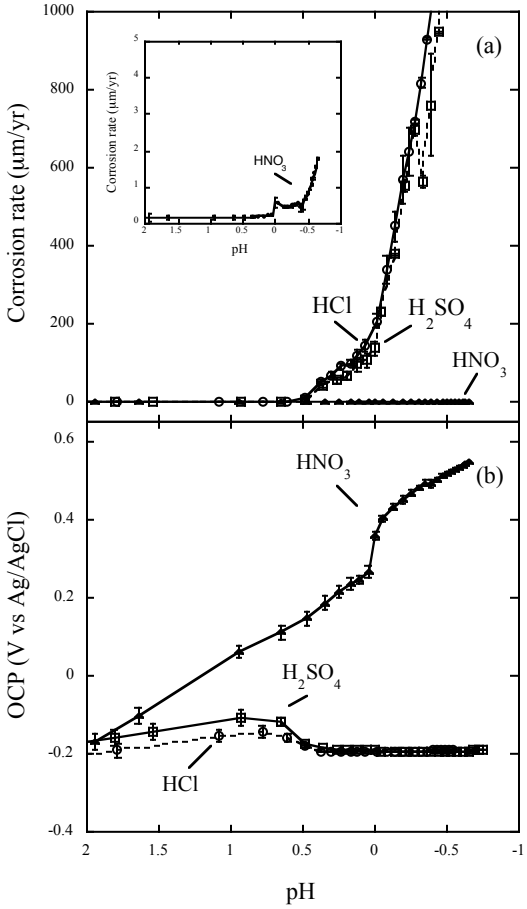
(a)
Corrosion rate (μm/yr)
HCl
H2SO4
HNO3
(b)
OCP (V vs Ag/AgCl)
HNO3
H2SO4
HCl
pH

Fig.4.

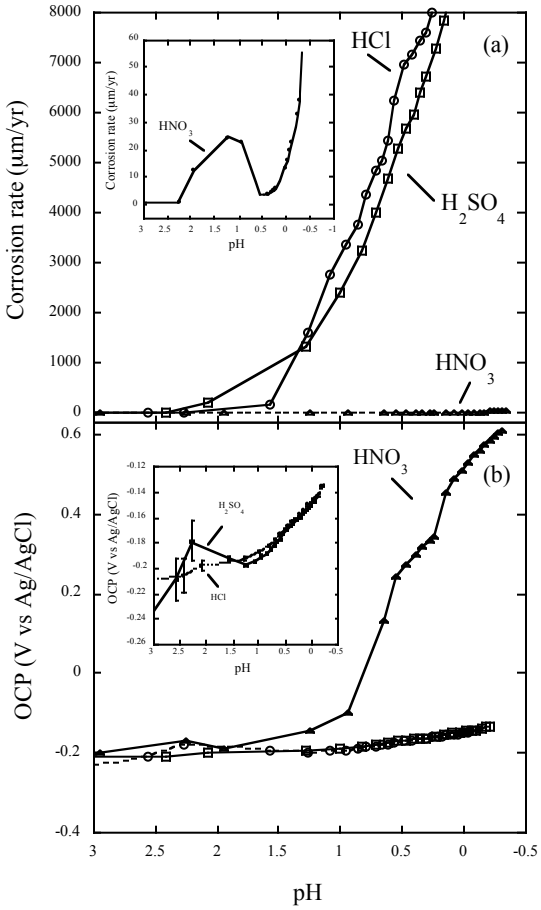
Corrosion rate (μm/yr)
HCl
(a)
H_2SO_4
HNO_3
Corrosion rate (μm/yr)
pH
OCP (V vs Ag/AgCl)
HNO_3
(b)
H_2SO_4
HCl
OCP (V vs Ag/AgCl)
pH
pH

Fig. 5.

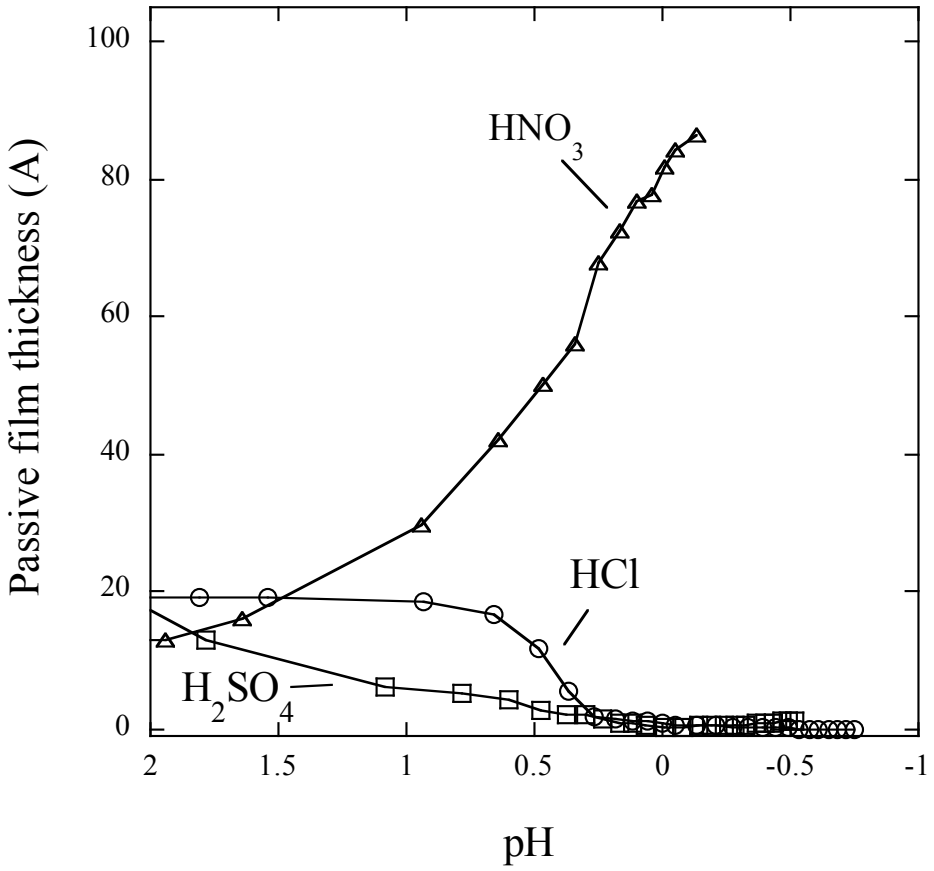
Passive film thickness (A)
100
80
60
40
20
0
2
1.5
1
0.5
0
-0.5
-1
pH
HNO3
HCl
H2SO4

Fig. 6.

(a) H_2SO_4

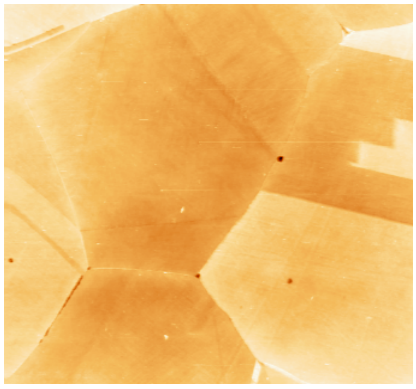

(b) HCl

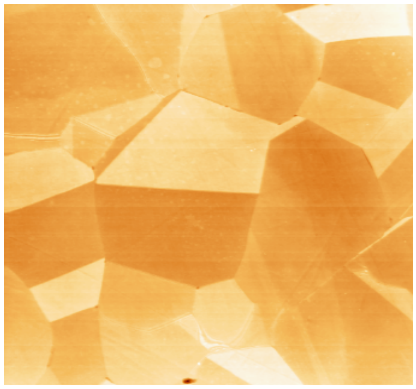

(c) HNO_3

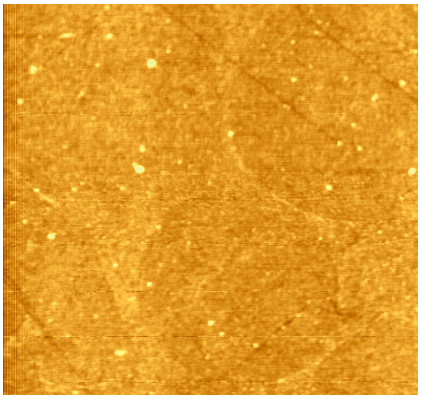

Fig. 7.

(a) H_2SO_4

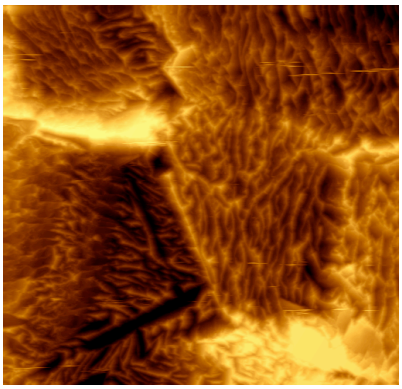

(b) HCl

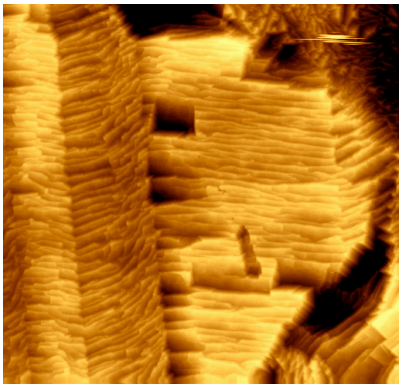

(c) HNO_3

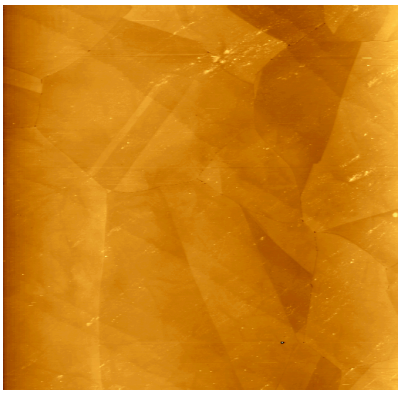

Fig. 8.

(a) H_2SO_4

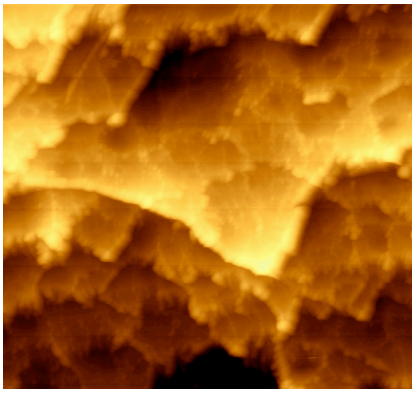

(b) HCl

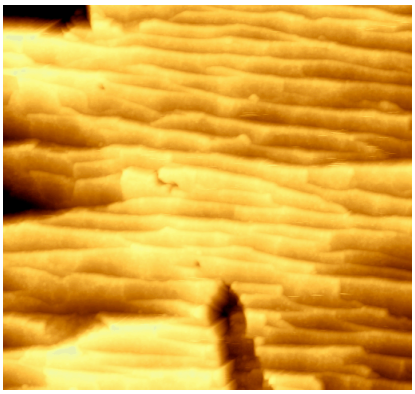

Fig. 9.

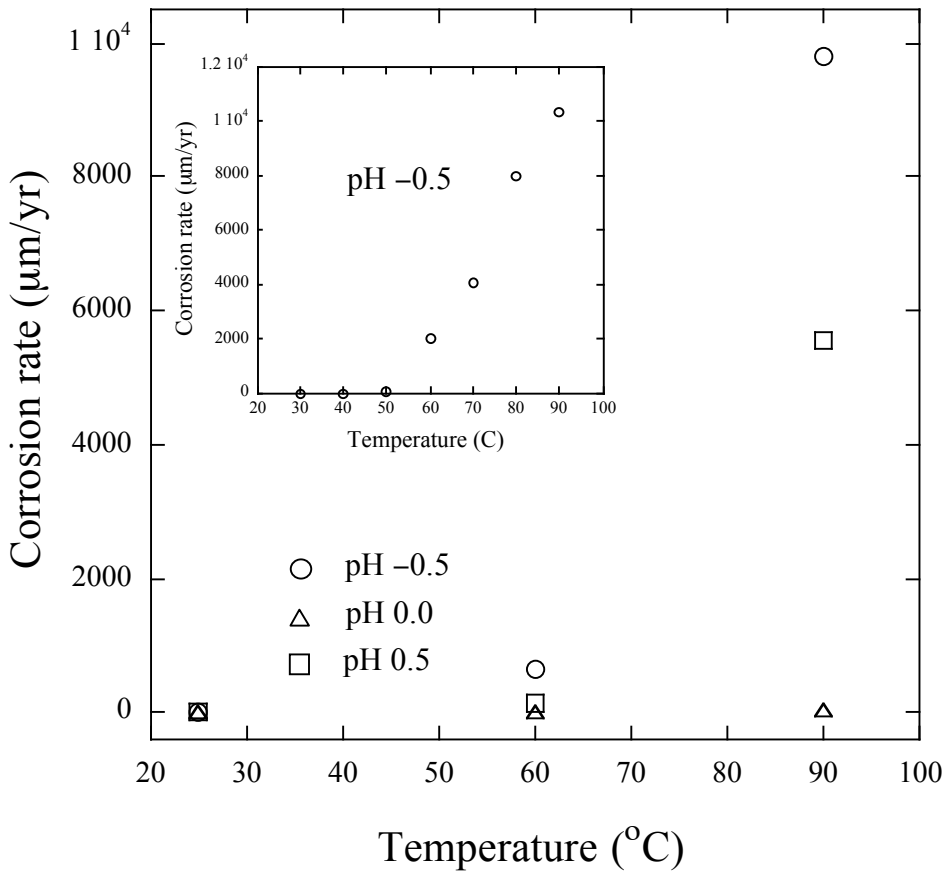
Corrosion rate (μm/yr)
Temperature (°C)
pH −0.5
pH 0.0
pH 0.5
Corrosion rate (μm/yr)
Temperature (C)
pH −0.5

Figure captions

1. Schematic of the acid titration experimental technique. After each acid titration, a two-hour open circuit potential (OCP) measurement is followed by linear polarization resistance (LPR) and electrochemical impedance spectroscopy (EIS) measurements.

2. (a) Corrosion rates and (b) open circuit potentials vs. pH for alloy 22 in hydrochloric, sulfuric and nitric acids with 1m NaCl at 60°C.

3. (a) Corrosion rates and (b) open circuit potentials vs. pH for alloy 22 in hydrochloric, sulfuric and nitric acids with 1m NaCl at 90°C.

4. (a) Corrosion rates and (b) open circuit potentials vs. pH for alloy 22 in hydrochloric, sulfuric and nitric acids with 4m NaCl at 90°C.

5. Passive film thickness of alloy 22 in hydrochloric, sulfuric and nitric acids with 1m NaCl at 60°C.

6. AFM topographic maps of the alloy 22 surface following titration in (a) sulfuric (100 μm x 100 μm), (b) hydrochloric (100 μm x 100 μm) and (c) nitric acids (10 μm x 10 μm) with 1m NaCl at 60°C.

7. 100 μm x 100 μm AFM topographic maps of the alloy 22 surface following titration in (a) sulfuric (100 μm x 100 μm), (b) hydrochloric (100 μm x 100 μm) and (c) nitric acids (100 μm x 100 μm) with 1m NaCl at 90°C.

8. 10 μm x 10 μm AFM micrographs of the topography of the alloy 22 surface following titration in (a) sulfuric and (b) hydrochloric acid solution with 1m NaCl at 90°C.

9. Corrosion rates vs. temperature for pH values of (circles) –0.5, (squares) 0.0 and (triangles) 0.5. (Inset) corrosion rates with temperature increments of 10°C showing the linear relationship between rates and temperature above a critical temperature (T_{crit} ~ 50°C).